

Received 2024-10-28
Revised 2024-11-29
Accepted 2024-12-07

Examination of A Novel Nanocomposer's Bioactivity for Use in Dentistry

Sarvenaz Amanolahi Baharvand ¹, Pardis Chaboki ², Fateme Pourhatami ³, Mohamad Milad Shirvandeji ⁴, Reza Yusofvand ⁵, Payam Ali -Khiavi ⁶, Mohammad Shabestari Khiabani ⁷✉, Khadije Yousefi ⁸, Paria Ganji Nataj ⁹, Paria Arjmandi Sarvestani ¹⁰, Sepideh Karkonshayan ¹¹, Reza Akhavan-Sigari ^{12, 13}

¹ Faculty of Pharmacy, Mazandaran University of Medical Sciences, Mazandaran, Iran

² School of Medicine, Shiraz University of Medical Sciences, Shiraz, Iran

³ Department of Basic Science, Faculty of Pharmacy, Pharmaceutical Sciences Branch, Islamic Azad University, Tehrani, Iran

⁴ Department of Microbiology, Faculty of Medicine, Arak University of Medical Sciences, Arak, Iran

⁵ Department of Exceptional Talents, Faculty of Medicine Sciences, Lorestan University of Medical Sciences, Khorramabad, Iran

⁶ School of Medicine, Tabriz University of Medical Sciences, Tabriz, Iran

⁷ Dentistry faculty, Tabriz University of Medical Sciences, Tabriz, Iran

⁸ Department of Materials Science and Engineering, School of Engineering, Yasouj University, Yasouj, Iran

⁹ Dalian Medical University, Dalian, China

¹⁰ Department of Biomedical Engineering, Faculty of Engineering, Zand Institute of Higher Education, Shiraz, Iran

¹¹ Student Research Committee, School of Medicine, Gonabad University of Medical Sciences, Gonabad, Iran

¹² Dreifaltigkeits-Hospital Lippstadt, Teaching Hospital of the University of Münster, Germany

¹³ Department of Health Care Management and Clinical Research, Collegium Humanum Warsaw Management University Warsaw, Poland

Abstract

The extended setting time of mineral trioxide aggregate (MTA) is one of its primary drawbacks. An alternative to MTA, Nano Fast Cement (NFC) is a novel nanocomposite with a quick setting time. In order to develop an exceptional dental filler, hydroxyapatite nanoparticles (NHA) were introduced to NFC to examine its impact on setting time, biocompatibility, and bioactivity qualities. X-ray diffraction, scanning electron microscopy, Gilmore needle, and MTT assay were used to evaluate the specimens with 0, 10, and 20 W% hydroxyapatite. The antibacterial evaluation was conducted using *Enterococcus faecalis* (PTCC 1394). Using phase and microstructural studies, the production of hydroxyapatite was discovered. Both 10 and 20 weight percent prime apatite enhanced the specimens' bioactivity and markedly decreased their toxicity behavior. More HA content resulted in greater bioactivity enhancement and toxicity decrease. These results suggest that the physical properties of NFC were not negatively impacted by the addition of NHA. In vitro, they enhanced the filler's bioactivity. [GMJ.2024;13:e3663] DOI:[10.31661/gmj.v13i.3663](https://doi.org/10.31661/gmj.v13i.3663)

Keywords: Nanocomposite; Nano Fast Cement; Setting Time; Nano Hydroxyapatite; Bioactivity

Introduction

In dental research, calcium silicate cements (CSCs), akin to mineral trioxide aggregate (MTA) [1], serve to mend deficiencies in tooth root sides and to complete root ends after procedures [2]. MTA was initially developed as

a root-end filling material due to its special therapeutic properties such as bioactivity [3], biocompatibility [4], and sealing ability [5]. Nonetheless [6], the challenges associated with it, including difficulty in handling, weakness, extended setting duration, color changes, and high expense [7], hinder its effectiveness

GMJ

Copyright© 2024, Galen Medical Journal.
This is an open-access article distributed
under the terms of the Creative Commons
Attribution 4.0 International License
(<http://creativecommons.org/licenses/by/4.0/>)
Email:gmj@salviapub.com



✉ **Correspondence to:**
Mohammad Shabestari Khiabani, Dentistry faculty, Tabriz University of Medical Sciences, Tabriz, Iran.
Telephone Number: 041 3335 7310
Email Address: Kkaa0585@gmail.com

for repair tasks [8, 9]. Ideally, a dental filler material should set quickly to prevent saliva from washing it away and reduce the risk of irritating oral tissues [5]. Prolonged setting time of MTA has been shown to cause various issues with dental treatment process management [10]. The normal setting time for MTA exceeds 2.5 to 3 hours under regular conditions [14]. Occasionally, achieving the final filling or cover for a tooth requires multiple attempts [11]. This shows that we need to create a new material made from calcium silicate and cement to make it set faster [12, 13]. New CSCs like Nano Fast Cement (NFC) from Sanat Avaran Vista, Iran [15], have been developed with an initial setting time of 5 minutes [16, 17]. NFC is a fast-setting CSC composed of zirconia oxide, silicon dioxide, and calcium dioxide [18]. In a recent laboratory experiment, NFC demonstrated a marginally shorter setting time at both the start and finish compared to Angelus MTA and Calcium-en-

riched cement (CEM). On the other hand, using calcium phosphate (CaP) as a material for bone grafts has had good results. When introduced into bone defects, calcium phosphates, including hydroxyapatite and beta-tricalcium phosphate (beta-TCP) [19], are safe for bodily use, stimulate bone formation, and facilitate healing [20].

Hydroxyapatite can serve as a scaffold for new bone formation and can enhance capillary [21], perivascular [22], and osteogenic cell growth in the recipient area [23]. An essential quality of retrofilling cement is its bioactivity [13], which enables the creation of a solid attachment to living tissue by producing a layer of hydroxyapatite [24-27]. However, the fundamental requirement for a material implanted in the human body is its biocompatibility [28]. The addition of hydroxyapatite to root canal sealers, dental materials, and tooth glues serves to reinforce them and enhance their effectiveness and biological response [29, 30]. NHA is a potential addition with attributes such as biocompatibility, bioactivity, and osteoconductivity [31, 32], making it a promising additive that could enhance the properties of NFC. This study seeks to determine the effects of integrating NHA with NFC in order to improve its biocompatibility, bioactivity, and antibacterial functions.

Table 1. The Different Compositions of NFC/NHA Nanocomposite

Materials	Powder composition	Hydration agent
NFCH0	100% NFC	water
NFCH10	90% NFC + 10%NHA	water
NFCH20	80% NFC + 20%NHA	water

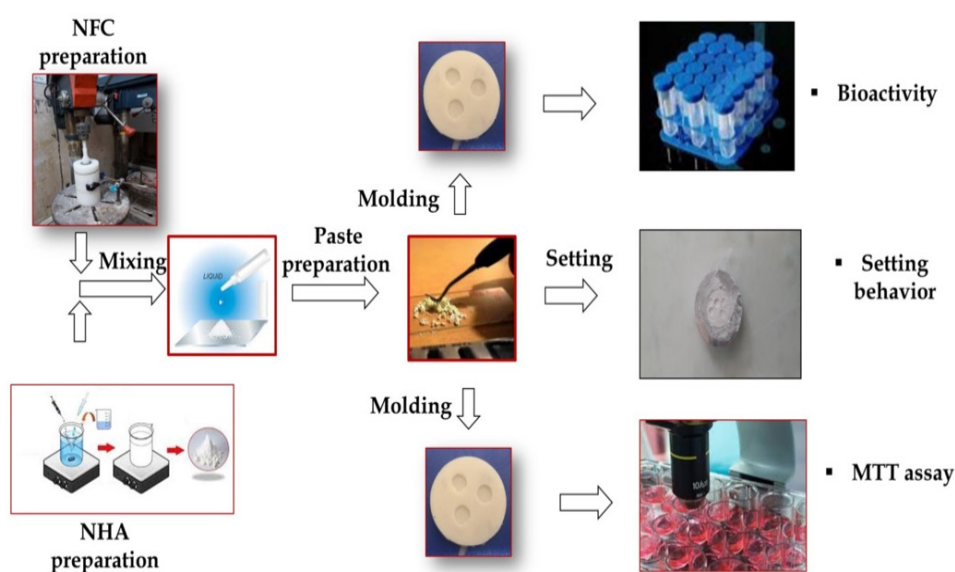


Figure 1. Material processing flow chart

Materials and Methods

Powder Preparation

The study utilized NFC as the main component, NHA as the bioactive element, and distilled water as the agent for hydration. The NHA&NFC powders were produced and characterized as detailed in previous studies [33, 34]. In brief, NHA was created through the blending of calcium nitrate tetrahydrate and phosphoric acid. Calcium nitrate tetrahydrate obtained from Sigma-Aldrich, USA, exhibited a purity of 99%. The phosphoric acid, which originated from Sigma-Aldrich, USA, exhibited a purity of 85%. The nano fact cement (Sanat Avaran Vista Co., Iran) with a particle size of 3453nm was reduced to 300nm through Wet-Stirred-Media-Milling over 15 hours. The composite NFC/NHA powder was created by blending NFC and NHA with 0, 10, and 20% of NHA powder for NFCH0, NFCH10, and NFCH20, respectively.

Paste Preparation

During this stage, the powders of the nano-

composite were mixed together with distilled water. Following this, the mixture was delicately stirred with a spatula for 30 seconds until a uniform and workable paste formed, which was then poured into a silicone mold. To identify the most effective composition for the produced calcium silicate nanocomposite, various compositions of the nanocomposite were prepared, as outlined in Table-1. The process for handling the materials is illustrated in Figure-1.

Phase Evaluation and Microstructural Characterization

The D-50 diffractometer Siemens model was used to determine the X-ray diffraction patterns, employing Cu-ka radiation with a 1.5 Å wavelength in the 2θ range of 20° - 60° . By employing JCPDS reference cards and Xpert high score software, we detected various patterns. A TESCAN-Vega 3 scanning electron microscope (SEM) was utilized to analyze the surface characteristics of samples before and after being submerged in SBF. To boost the efficiency of electricity conduction, a slim coat-

Table 2. Ion Concentrations (mM) in Artificial Body Fluid Versus Blood Plasma Levels [22]

Formulation	Na ⁺	K ⁺	Ca ²⁺	Mg ²⁺	Cl ⁻	HCO ³⁻	HPO ₄ ²⁻	SO ₄ ²⁻
Human blood plasma	142	5	2.5	1.5	103	27	1	0.5
SBF	142	5	2.5	1.5	147.8	4.2	1	0.5

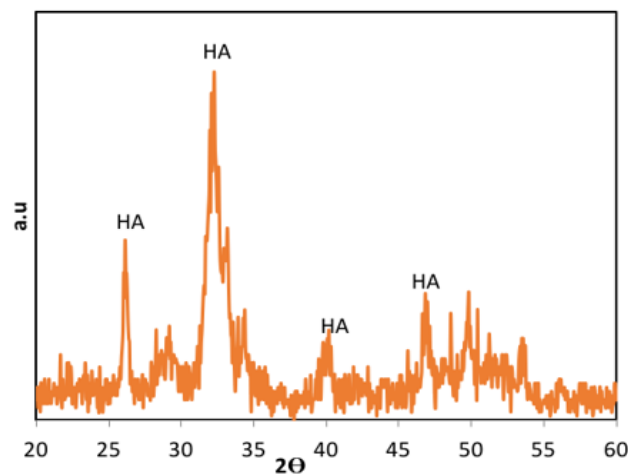


Figure 2. XRD patterns of NHA powder

ing of carbon was added to the samples. The analysis of the samples was conducted with a scanning electron microscope, operating at a voltage of 15 kV.

Setting Time Evaluation

The measurement of the NFC's setting times was conducted following the standards outlined in ISO 6876/2012. The experimental mixtures were combined and transferred into a circular stainless-steel mold that has a width of 5 mm and a height of 10 mm. Once mixed, the samples were positioned in an incubator maintained at 37 degrees Celsius and 95% relative humidity. A 1 mm wide flat tip was employed, and it had a weight of 400 grams. It was firmly positioned straight down onto the

tested material's surface. This repeated itself every minute. The time for final setting was logged when the needle no longer created a mark.

Handling Properties

The samples' handling characteristics were evaluated with a texture analyzer (CT3, Brookfield, Middleboro, USA) equipped with a 4.5 kg load sensor. Each sample was compressed using a tool measuring 5 mm in diameter and having a volume of one cubic centimeter. This was executed with a speed rate of 0.02 mm per second after mixing the sample. By measuring the force necessary to compress the material to a designated depth, we were able to evaluate how manageable it is.

Table 3. XRD Peaks of Ingredients of Cement

Compound	1th peak	2th peak	3th peak	4th peak	5th peak	6th peak
C ₃ S	29.51°	32.70°	34.41°	41.48°	51.70°	
C ₂ S	31.98°	32.37°	40.55°			
Ca (OH) ₂	34.1°	47.63°				
Zirconium oxide	27.37°	33.40°	49.3°,50			
C-S-H	26.59°	29.36°	30.92°	47.73°	50.52°	
Hydroxyapatite	25.88°	31.77°	32.90°	39.79°	46.69°	49.49°

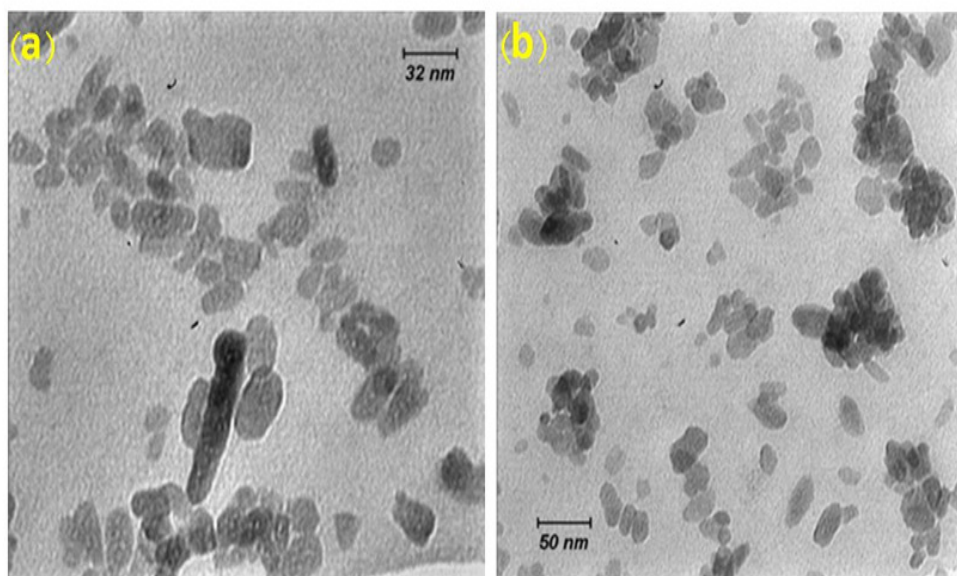


Figure 3. TEM images of NHA powders a) 32 nm resolution b) 50 nm resolution

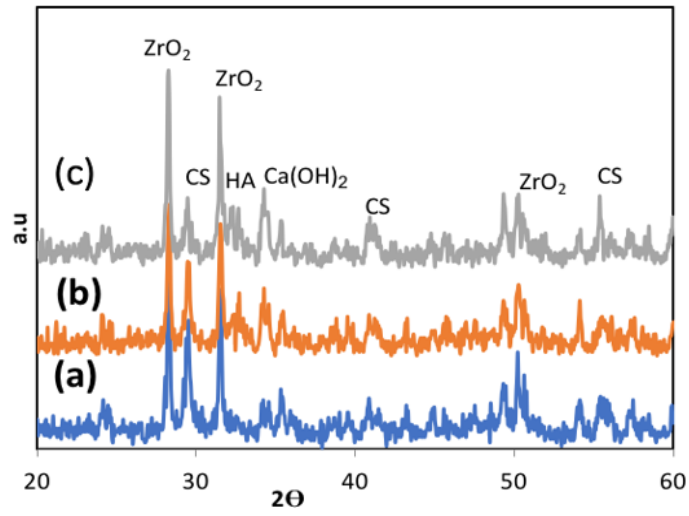


Figure 4. XRD patterns of NFCH0, NFCH10, and NFCH20 before soaking in SBF

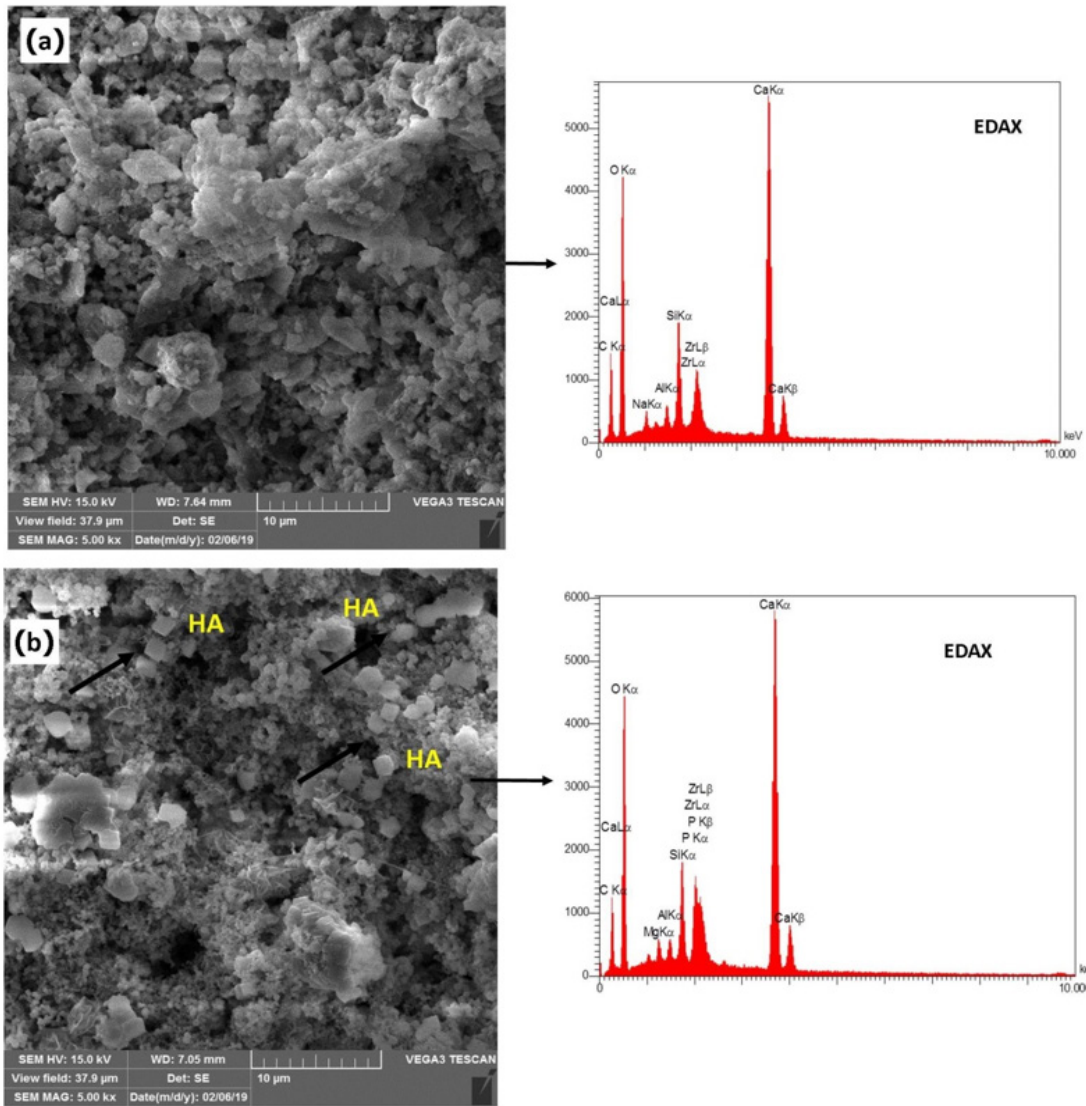


Figure 5. SEM & EDAX of NFCH0 and NFCH20 the distribution of NHA particles present in NFC

Bioactivity Evaluation

The bioactivity was assessed following the guidelines outlined in ISO 23317 [36]. A little segment, measuring 10 mm across and 2 mm long, was fabricated and then immersed in a fluid that imitates body fluids for 14 days once it had set. Simulated body fluid (SBF) is a liquid composed of particles similar to those found in human blood. It is buffered to a pH of 7.40 at physiological temperature using HEPES/NaOH [37, 38]. The chemical composition of SBF can be found in Table-2.

Statistical Analysis

In the present study, SPSS IBM subsidized software was used to analyze the data. To evaluate the results of biological experiments, the data was displayed in each group as mean \pm standard deviation. A significant difference between mean groups was analyzed by one-way ANOVA analysis and then Tukey test. In all experiments, an average of 3 measurements was used for each group, and a significant level in all statistical tests (P) was considered less than 0.05.

Results & discussion

Characterization of Synthesized Powders and Cement Pastes

In the present study, Figure-2 depicts the XRD patterns of NHA powder, exhibiting the characteristic peaks of hydroxyapatite and indicating the absence of impurities in the pro-

duced hydroxyapatite powder. Furthermore, Figure-3 displays the transmission electron microscopy images of the synthesized hydroxyapatite powder, revealing that the hydroxyapatite nanoparticles measure between 20 and 50 nm in size. This powder was utilized in the fabrication of a calcium silicate nanocomposite containing hydroxyapatite, and its impact on NFC properties was examined. Figure-4 displays the X-ray diffraction (XRD) patterns for NFCH0, NFCH10, and NFCH20. These patterns are consistent with the samples before their exposure to the simulated body fluid (SBF) solution. In Table-3, the significant peaks corresponding to the different compounds can be observed. The primary components of NFC consist of tricalcium silicate (C3S), dicalcium silicate (C2S), tricalcium aluminate (C3A), along with zirconium oxide. The addition of water results in a slight reduction of tricalcium silicate and dicalcium silicate, while it leads to the formation of calcium silicate hydrate (C-S-H) and calcium hydroxide (Ca(OH)₂). The spectrum exhibits an additional peak in the NFCH10 and NFCH20 specimens at 31.7 and 32.5°, respectively. These peaks correspond to the hydroxyapatite, which was incorporated at 10 and 20 weight percent into NFC to enhance the cement's bioactivity properties Table-3. Figure-5 displays the SEM images of the NFCH0 and NFCH20 samples, revealing fine particles dispersed on the CSH surface. Examination of the X-ray energy distribution of these parti-

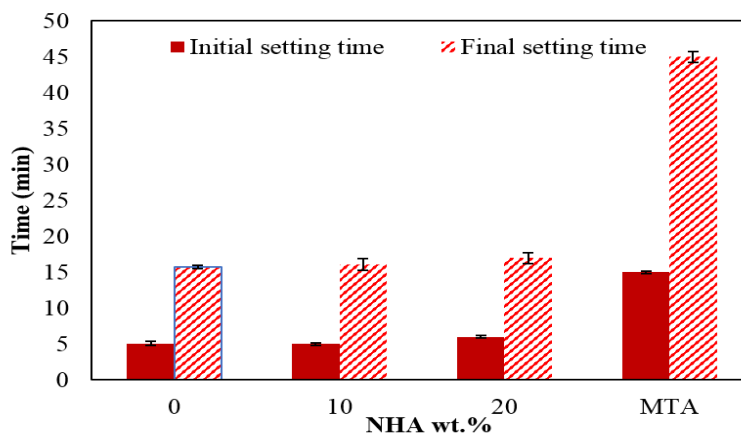


Figure 6. The effect of NHA on the rapidity of NFC initialization

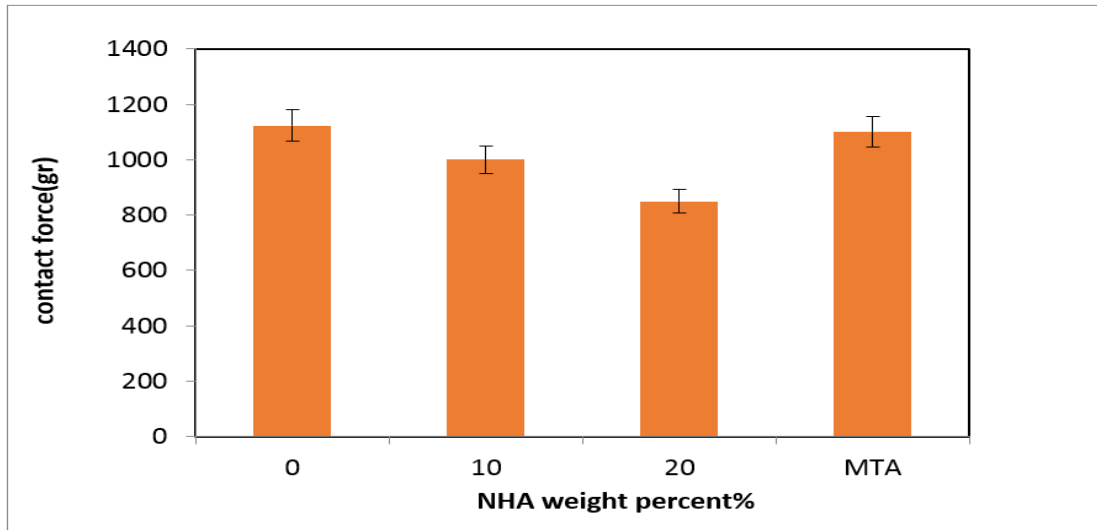


Figure 7. The effects of NHA on the handling properties of the NFC

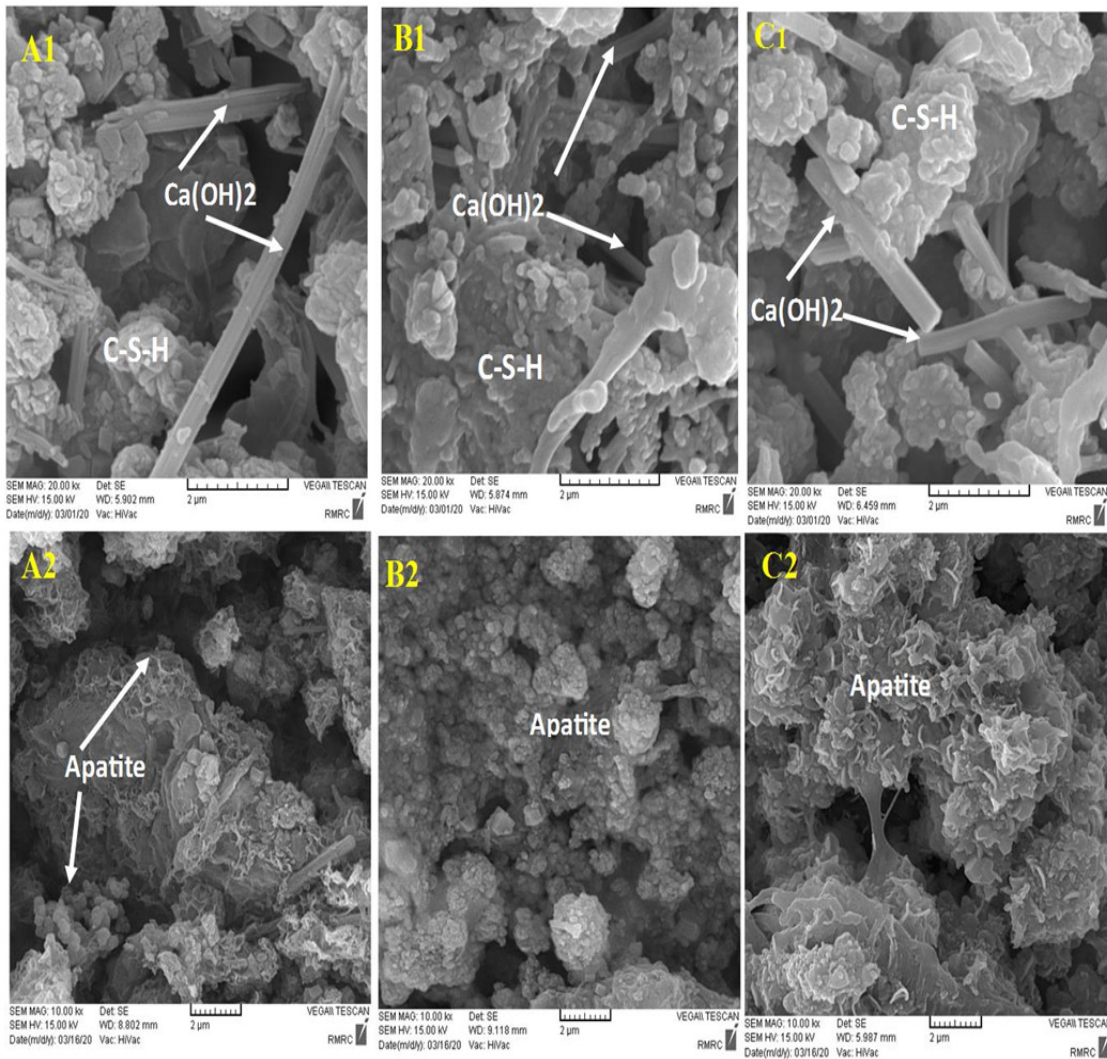


Figure 8. SEM image of the sample before soaking in SBF (A1) NFCH0, (B1) NFCH10 (C1) NFCH20 after soaking in SBF for 14 days (A2) NFCH0 (B2) NFCH10 (C3) NFC20

cles indicates that they consist of hydroxyapatite. Calcium and phosphorus were found in the X-ray analysis of the material, attributed to the presence of apatite in the NFC.

The Effect of Nano-hydroxyapatite on the Setting Time of NFC

The NFC consists of hydrophilic particles that solidify upon exposure to moisture [15]. This substance offers an alternative to MTA, which has a lengthy setting time that is not ideal for clinical use [39]. The setting characteristics of NFC are examined in this section, including the influence of adding NHA on the setting time. The structure and hydration of NFC result from a series of intricate reactions. The starting and finishing times for each of the different mixtures are displayed in Figure-6. The initial setting time for NFCH0 was approximately 5 minutes, with a final setting time of 15.75 minutes. MTA is a widely used dental sealer, with a setting time of 2-3 hours, The speed is considerably slow, which can result in various health concerns [40]. The findings indicate that by using pure NFC, the setting time can be reduced by 7.5-11 times compared to MTA. The rise in the amount of NHA results in a minimal change in the initial and final setting times of NFC, as depicted in Figure-6. Hydroxyapatite nanoparticles, which are calcium phosphate, do not disrupt hydration reactions and therefore have little

impact on the setting time. Any slight increase in setting time may have been influenced by the powder/liquid ratio, given that samples containing NHA required a greater amount of water to achieve a suitable consistency for clinical purposes, consequently leading to an increase in the setting timeb [41-46].

Handling Properties

The handling properties were assessed by measuring the maximum contact force needed to compress prepared pastes using a 5 mm diameter probe to a depth of 4 mm. Figure-7 compares the contact force of samples prepared with 0, 10, and 20 wt% NHA. The figure indicates that the contact force decreases for samples containing 10 and 20 wt% NHA in the NFC paste. Specifically, the contact force for the sample with 0 wt% NHA (NFC0) is 1123 gr, which decreases to 800 gr when 20 wt% NHA is used in the NFC20. The demand for advanced dental materials has led to the exploration of nanocomposites, which offer enhanced mechanical properties and bioactivity. Understanding the thermal behavior of these materials under various conditions is crucial for their application in dentistry [41-46].

In vitro Bioactivity Test

The nanocomposite's bioactivity was assessed through in vitro tests involving immersion in

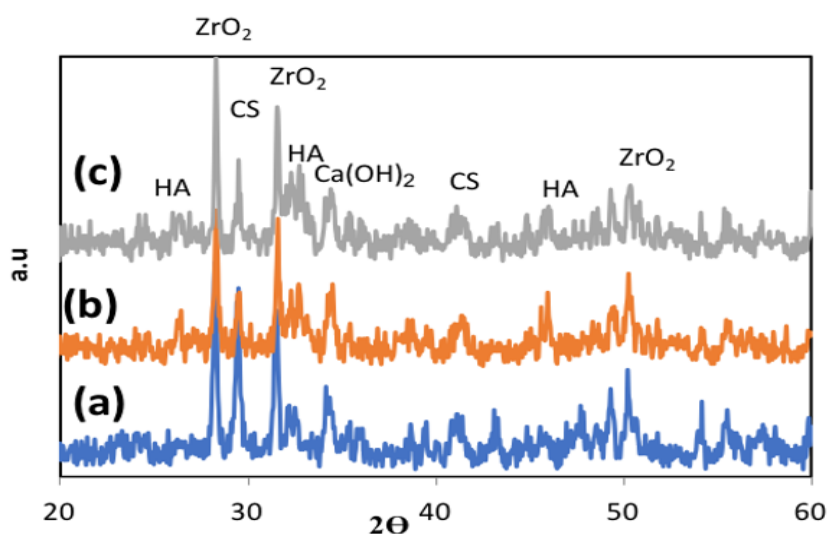


Figure 9. XRD patterns of a)NFCH0 b)NFCH10c) NFCH20 after soaking in SBF

SBF at 36.5 °C for 14 days. Following this immersion, XRD and SEM analysis were conducted to examine the formation of apatite on the nanocomposite surfaces. The presence of secondary apatite on the surfaces after exposure to SBF provides insight into its bioactivity under *in vitro* conditions, as stated in the literature. SEM and EDAX images of three different samples before and after immersion in SBF are shown in Figure-8. The microstructure of NFCH0, NFCH10, and NFCH20 before immersion is depicted in Figure-8(A1, B1, C1), displaying a composition of CSH matrix, calcium hydroxide crystals, and some pores resulting from hydration reactions. Figure-8 (A2, B2, C2) illustrates the microstructure of NFCH0, NFCH10, and NFCH20 after 14 days of immersion in SBF, revealing a notable development of apatite on the cement surfaces. Notably, NFCH10 and NFCH20 exhibited greater homogeneity and uniformity with fewer porosities compared to the NHA-

free sample (NFCH0), and the formation of hydroxyapatite crystals was more pronounced on their surfaces. Understanding the development of apatite on cement is crucial for assessing its compatibility with living tissues and its possible applications in dentistry. The XRD spectrum of hydrated samples after SBF immersion is presented in Figure-9, indicating that the spectrum of NFCH0 after soaking in SBF is similar to the spectrum of NFCH0 before soaking, with the difference being the detection of the hydroxyapatite spectrum at 31.7&32.5°. The presence of these peaks serves as evidence of hydroxyapatite formation on the cement surfaces, confirming its bioactivity. Interestingly, the spectrum of samples NFC10 and NFC20 after soaking in solution is similar to that of NFC0, but the hydroxyapatite peaks appear more prominently, indicating that the addition of hydroxyapatite to the primary cement powders significantly enhances the cement's bioactivity, which is

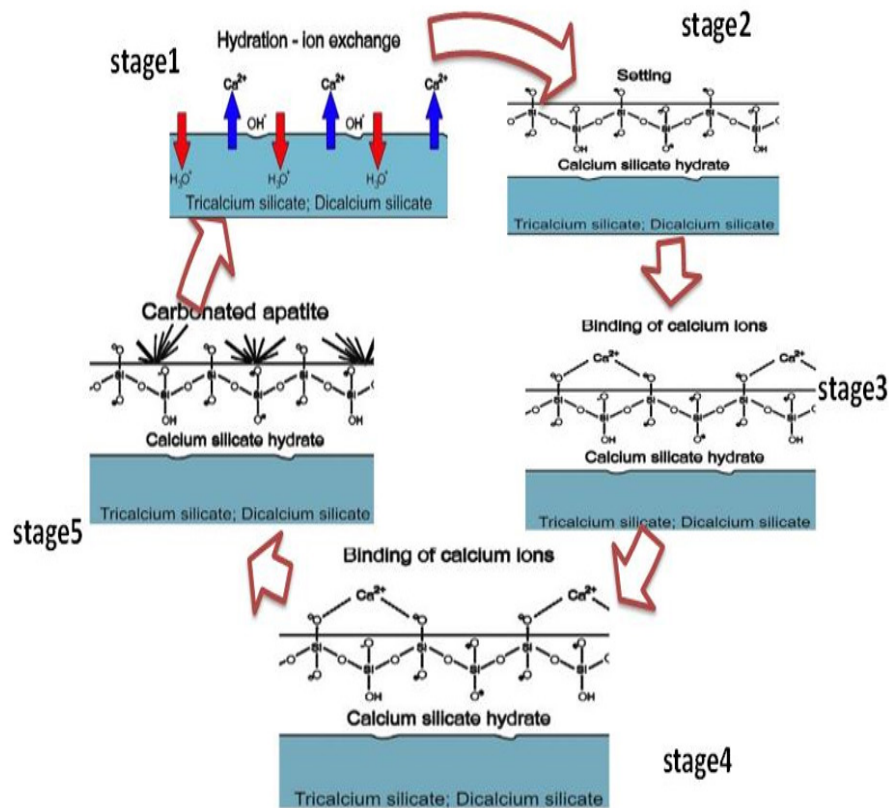
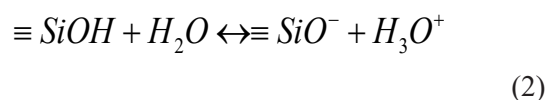


Figure 10. Schematic of the five concurrent stages of activities leading to the realization of NFC's bioactivity *in vitro* after the latter is immersed in virtual body fluid. ACP: amorphous phosphate calcium.

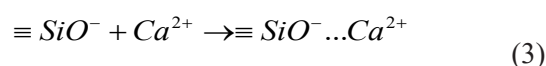
suitable for dental purposes [47-51]. In order to facilitate comparisons, we'll reference a comparable sequence of events in this discussion. These stages are depicted in an uncomplexed diagram included in Figure-10.

The functioning of the mechanism can be described in the following manner:

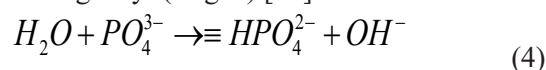
Once NFC comes into contact with SBF, a boundary forms between the cement and solution, leading to hydrolysis (stage 1) [52, 53]. Ion exchanges commence between hydration products or C3S and C2S, with Ca²⁺ from the cement swapping with H⁺ from the aqueous solution to establish a solid-liquid interface. This interaction between Ca²⁺ ions and hydroxyl ions from water generates an alkaline environment (stage 2). By increasing the OH⁻ concentration in the solution, cation exchange leads to the coating of calcium silicate particle surfaces with hydroxyl ions [54]. The process of hydrolysis produces the SiO₄⁻ grouping, aiding in the development of calcium silicate hydrate on cement surfaces in basic environments. This structure has no clear shape [55]. The structure of calcium silicate hydrate consists of a water-saturated gel formed by minuscule, porous particles that house silanol or Si-OH groups. Subsequently, in a basic environment, the Si-OH group within the calcium silicate hydrate releases a proton (H⁺). Through this process, a surface is generated that carries a negative charge due to the presence of a SiO⁻ group (Stage 3) [56]: that carries a negative charge due to the presence of a SiO⁻ group (Stage 3) [56]:



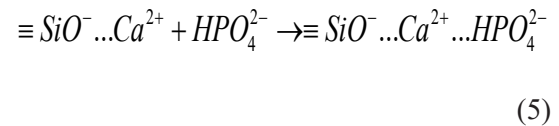
The negative group formed attracts positive calcium ions released into the solution due to electrical forces, resulting in an increased concentration of positive ions on the cement's surface [57]:



It consists of two layers that possess opposing charges, enabling other materials to adhere to its surface. Alternatively, the SBF solution comprises PO₄³⁻ that breaks apart in the following way: (stage4) [35]:



The addition of calcium silicate to a phosphate-rich solution, referred to as SBF, that has disassembled HPO₄²⁻ promotes interactions between HPO₄²⁻ and Ca²⁺ on the surfaces of the cement. As a result of this process, apatite is formed unevenly (stage5) [58]:



Based on the SEM&EDAX and XRD findings of NCFH0, NFCH10, and NFCH20, it can be observed that the bioactivity of NFCH10 and NFCH20 surpasses that of NCFH0. This is attributed to the fact that the bioactivity of the degradable material is directly linked to the speed at which the ionic products are released from the corroding surface in a physiological solution [30]. NFCH20 and NFCH10 exhibit a higher quantity of hydroxyapatite nanoparticles in comparison to NCFH0. Upon immersion in the SBF solution, the hydroxyapatite nanoparticles migrate into the solution, leading to an increase in the concentration of calcium and phosphorus ions in the solution. The calcium, phosphate, and silicate ions released from the surface of the calcium silicate nanocomposite eventually react with the ions coming from SBF, resulting in the formation of insoluble salts such as hydroxyapatite on the surface of the cement. The elevation in the concentration of calcium and phosphorus ions accelerates the formation of hydroxyapatite on the sample surface, signifying an enhancement in bioactivity [59-63]. The heightened ionic activity of NCH20, in comparison to NCH10, led to a greater amount of apatite formation on the sample surfaces, which is attributed to the increased quantity of primary apatite in the microstructure.

Conclusion

This study focused on assessing the effects of integrating hydroxyapatite nanoparticles (NHA) into NFC regarding the time required for it to set and its potential for supporting biological life. This aims to generate suitable filler material. Research into the various phases revealed that a compound known as apatite developed on samples that had been immersed in simulated body fluid (SBF) for a

duration of 14 days. This was additionally assessed and corroborated through observation of the microstructure. This indicates that NFC is beneficial for health and safe for utilization. The presence of 10% and 20% primary apatite in the samples increased bioactivity and notably decreased sample cytotoxicity. The

nanocomposite NFC/NHA exhibited positive biological properties and could potentially be a safe option for restorative treatment.

Conflict of Interest

None.

References

1. Lee sj, Monsef M, Torabinejad M. Sealing ability of a mineral trioxide aggregate for repair of lateral root perforations. *Journal of endodontics*. 1993;19(11):541-544.
2. Mousavi SM, et al. Asymmetric Membranes: A Potential Scaffold for Wound Healing Applications. *Symmetry*. 2020;12(7):1100.
3. Parirokh M, Torabinejad M. Mineral trioxide aggregate: a comprehensive literature review-Part III: Clinical applications, drawbacks, and mechanism of action. *J Endod*. 2010;36(3): 400-13.
4. Camilleri j, Sorrentino f, Damidot D. Investigation of the hydration and bioactivity of radiopacified tricalcium silicate cement, Biodentine and MTA Angelus. *Dental Materials*. 2013;29(5):580-593.
5. Takmil F, Esmaeili H, Mousavi SM, Hashemi SA. Nano-magnetically modified activated carbon prepared by oak shell for treatment of wastewater containing fluoride ion. *Advanced Powder Technology*. 2020;31(8):3236-3245.
6. Mousavi sm, et al. Data on cytotoxic and antibacterial activity of synthesized Fe₃O₄ nanoparticles using *Malva sylvestris*. *Data in brief*. 2020;28:104929.
7. Meng D, Erol M, Boccaccini AR. Processing technologies for 3D nanostructured tissue engineering scaffolds. *Advanced engineering materials*. 2010 Sep;12(9):B467-87.
8. Malkondu o, Karapinar Kazandag m, Kazazoglu e. A review on biodentine, a contemporary dentine replacement and repair material. *Biomed Res Int*. 2014;2014: 160951.
9. Darvell b, Wu r. MTA"—an hydraulic silicate cement: review update and setting reaction. *Dental Materials*. 2011;27(5):407-422 .
10. Ber bs, Hattonn jf, Stewart gp. Chemical modification of ProRoot MTA to improve handling characteristics and decrease setting time. *Journal of endodontics*. 2007;33(10):1231-1234.
11. Mousavi Sm, et al. Recent advancements in polythiophene-based materials and their biomedical, geno sensor and DNA detection. *International Journal of Molecular Sciences*. 2021;22(13):6850.
12. Mousavi sm, et al. Gold nanostars-diagnosis, bioimaging and biomedical applications. *Drug metabolism reviews*. 2020;52(2):299-318.
13. Mousavi sm, et al. Multifunctional gold nanorod for therapeutic applications and pharmaceutical delivery considering cellular metabolic responses, oxidative stress and cellular longevity. *Nanomaterials*. 2021;11(7):1868.
14. Kogan P, He j, Glickman gn, Watanabe i. The effects of various additives on setting properties of MTA. *Journal of endodontics*. 2006;32(6):569-572.
15. Sanaee mr, et al. The influence of particle size and multi-walled carbon nanotube on physical properties of mineral trioxide aggregate. *Materials Research Express*. 2019;6(6):065413.
16. Gholami a, et al. 3D nanostructures for tissue engineering, cancer therapy, and gene delivery. *Journal of Nanomaterials*. 2020; 2020(1):1852946.
17. Yousefi k, Daneshmanesh h. Optimization of physical and mechanical properties of calcium silicate nanocomposite by Taguchi method. *journal of New Materials*. 2020;11(39):77-90.
18. Yousefi k, Manesh hd, Khalifeh a, Moazami f, Sanaee m. Nanocement/poly (vinyl alcohol) composites for endodontic applications. *Materials Chemistry and Physics*. 2020;254 :123337.
19. Horowitz ra, Mazor z, Miller rj, Krauser j, Prasad hs, Rohrer md. Clinical evaluation alveolar ridge preservation with a beta-tricalcium phosphate socket graft. *Compend Contin Educ Dent*. 2009;30(9):588-590.
20. Reynolds ma, et al. Periodontal regeneration—intrabony defects: a consensus report from the AAP Regeneration Workshop. *Journal of periodontology*. 2015;86:S105-S107.

21. Hoexter dl. Bone regeneration graft materials. *Journal of oral implantology*. 2002;28(6): 290-294.
22. Sammarco vj, Chang l. Modern issues in bone graft substitutes and advances in bone tissue technology. *Foot and ankle clinics*. 2002;7(1):19-41.
23. Mousavi sm, et al. Renewable Carbon Nanomaterials: Novel Resources for Dental Tissue Engineering. *Nanomaterials*. 2021;11(11):2800.
24. Westhauser f, et al. Favorable angiogenic properties of the borosilicate bioactive glass 0106-B1 result in enhanced in vivo osteoid formation compared to 45S5 Bioglass. *Biomaterials science*. 2019;7(12):5161-5176.
25. Mousavi sm, et al. Bioactive Agent-Loaded Electrospun Nanofiber Membranes for Accelerating Healing Process: A Review. *Membranes*. 2021;11(9):702.
26. Ashoori y, et al. Development and In Vivo characterization of probiotic lysate-treated chitosan Nanogel as a novel biocompatible formulation for wound healing. *BioMed Research International*. 2020;2020(1):8868618.
27. Seyedmajidi s, Rajabnia r, Seyedmajidi m. Evaluation of antibacterial properties of hydroxyapatite/bioactive glass and fluorapatite/bioactive glass nanocomposite foams as a cellular scaffold of bone tissue. *Journal of laboratory physicians*. 2018;10(3):265-270.
28. Black j. *Biological performance of materials. fundamentals of biocompatibility*: Crc Press; 2005.
29. Collares f, Leitune v, ostirolla f, Trommer r, Bergmann c, Samuel s. Nanostructured hydroxyapatite as filler for methacrylate-based root canal sealers. *International Endodontic Journal*. 2012;45(1):63-67.
30. Leitune vcb, Collares fm, Trommer rm, Andrioli dg, Bergmann cp, Samuel smw. The addition of nanostructured hydroxyapatite to an experimental adhesive resin. *Journal of Dentistry*. 2013;41(4): 321-327.
31. Alsters pl, et al. Fine-tuning and recycling of homogeneous tungstate and polytungstate epoxidation catalysts in Mechanisms in Homogeneous and Heterogeneous Epoxidation Catalysis. Elsevier. 2008:415-428.
32. Yousfi kh, Zabarjad sm, Mojtaba s . Optimization of Taguchi statistical barouch test conditions for the production of hydroxyapatite nanoparticles by sol-gel method. *Modern Materials Scientific-Research Quarterly*. 2014;4(15):1-10.
33. Yousefi K, Zebarjad Sm, Vahdati KJ. Comparison Of Poly-Ethylene Glycol Effect on Hydroxyapatite Morphology. Produced Into Different Method: Sol-Gel and Precipitation; 2015.
34. Ayaz M, Ghasemi FA, Rahimloo VP, Menbari S. Multi-response optimization of the mechanical properties of PP/talc/ CaCO₃ ternary nanocomposites by the response surface methodology combined with desirability function approach. *Journal of Elastomers & Plastics*. 2018:0095244318819184.
35. International Standardization Organization. "ISO 6876, Dental root canal sealing materials."; 2012.
36. Standard b. BS ISO 23317: 2012 Implants for surgery," vitro evaluation for apatite-forming ability of implant materials. Switzerland: BSI Standards Limited; 2012.
37. Kokubo t, Takadama h. How useful is SBF in predicting in vivo bone bioactivity. *Biomaterials*. 2006;27(15): 2907-2915.
38. Abbaszadegan a, Gholami a, Mirhadi h, Saliminasab m, Kazemi a, Moein mr. Antimicrobial and cytotoxic activity of *Ferula gummosa* plant essential oil compared to NaOCl and CHX: a preliminary in vitro study. *rde*. 2014;40(1):50-57.
39. Roberts hw, Toth jm, Berzins dw, Charlton dg. Mineral trioxide aggregate material use in endodontic treatment: a review of the literature. *Dental materials*. 2008; 24(2):149-164.
40. Kamali a, Dezfuli sn, Javadpour s. Fabrication of MTA-like cements and their mechanical, handling, and setting properties in relation to the choice of setting solution. *Journal of the Australian Ceramic Society*. 2017;53(2):733-741.
41. Sohrabi N, Haddadvand R, Nabi H. Numerical investigation of the effect of fluid nanohybrid type and volume concentration of fluid on heat transfer and pressure drop in spiral double tube heat exchanger equipped with innovative conical turbulator. *Case Studies in Thermal Engineering*. 2024 Aug 1; 60:104751.
42. Torabinejad m ,Parirokh m. Mineral trioxide aggregate: a comprehensive literature review—part II: leakage and biocompatibility investigations. *Journal of endodontics*. 2010;36(2):190-202.
43. Nafissi N, Heiranizadeh N, Shirinzadeh-

- Dastgiri A, Vakili-Ojarood M, Naseri A, Danaei M, Saberi A, Aghasipour M, Shiri A, Yeganegi M, Rahmani A. The Application of Artificial Intelligence in Breast Cancer. *EJMO*. 2024;8(3):235-44.
44. Mohammadi V, Shahbad R, Hosseini M, Gholampour MH, Shiry Ghidary S, Najafi F, Behboodi A. Development of a two-finger haptic robotic hand with novel stiffness detection and impedance control. *Sensors*. 2024 Apr 18;24(8):2585.
 45. Mousavi sm, et al. Green synthesis of supermagnetic Fe₃O₄-MgO nanoparticles via Nutmeg essential oil toward superior anti-bacterial and anti-fungal performance. *Journal of Drug Delivery Science and Technology*. 2019;54:101352.
 46. Arvand m, Hemmati s. Analytical methodology for the electro-catalytic determination of estradiol and progesterone based on graphene quantum dots and poly (sulfosalicylic acid) co-modified electrode. *Talanta*. 2017;174:243-255.
 47. Mousavi sm, et al. Recent Progress in Chemical Composition, Production, and Pharmaceutical Effects of Kombucha Beverage: A Complementary and Alternative Medicine. *Evidence-Based Complementary and Alternative Medicine*. 2020;2020(1): 4397543.
 48. Ahmadi s, Fazilati m, Mousavi sm, Nazem h. Anti-bacterial/fungal and anti-cancer performance of green synthesized Ag nanoparticles using summer savory extract. *Journal of Experimental Nanoscience*. 2020;15(1): 363-380.
 49. Natu vp, et al. Bioactivity, physical and chemical properties of MTA mixed with propylene glycol. *J Appl Oral Sci*. 2015;23(4):405-11.
 50. Haddadvand R, Sohrabi N, Yan TX, Nadalinia F, Karouei SH. Numerical study on the influence of flow direction and fluid type on heat transfer and pressure drop in a two-tube spiral heat exchanger with innovative conical turbulators. *Case Studies in Thermal Engineering*. 2024 Sep 1;61:104933.
 51. Lin mc, Chen cc, Wu it, Ding sj. Enhanced antibacterial activity of calcium silicate-based hybrid cements for bone repair. *Materials Science and Engineering*. 2020; 110:110727.
 52. Hernández ml, Ruiz je, Ramos ap, Estévez gf, Sánchez ca. PMMA/Ca²⁺ bone cements Hydrolytic properties and bioactivity. *Polímeros*. 2012;22(4):390-394.
 53. Panahi f, Rabiee sm, Shidpour r. Synergic effect of chitosan and dicalcium phosphate on tricalcium silicate-based nanocomposite for root-end dental application. *Materials Science and Engineering*. 2017;80:631-641.
 54. Huan z, Chang j. Self-setting properties and in vitro bioactivity of calcium sulfate hemihydrate-tricalcium silicate composite bone cements. *Acta Biomater*. 2007;3(6):952-60.
 55. Davies je. Bone bonding at natural and biomaterial surfaces. *Biomaterials*. 2007;28(34):5058-5067.
 56. Labbez c, Jönsson b, Pochard i, Nonat a, Cabane b. Surface charge density and electrokinetic potential of highly charged minerals: experiments and Monte Carlo simulations on calcium silicate hydrate. *The Journal of Physical Chemistry*. 2006;110(18):9219-9230.
 57. Liu x, Ding c, Chu pk. Mechanism of apatite formation on wollastonite coatings in simulated body fluids. *Biomaterials*. 2004;25(10):1755-1761.
 58. Dey a, et al. The role of prenucleation clusters in surface-induced calcium phosphate crystallization. *Nature materials*. 2010;9(12):1010-1014.
 59. Siriphannon p, Kameshima y, Yasumori a, Okada k, Hayashi s. Influence of preparation conditions on the microstructure and bioactivity of α -CaSiO₃ ceramics: Formation of hydroxyapatite in simulated body fluid. *Journal of biomedical materials research*. 2000;52(1):30-39.
 60. Mohamed kr, Beherei hh, El-Rashidy zm. In vitro study of nano-hydroxyapatite/chitosan-gelatin composites for bio-applications. *Journal of Advanced Research*. 2014;5(2):201-208.
 61. Mohammadi AT, Marvast AF, Pishkari Y, Aghaei F, Janbozorgi A, Bozorgi AJ, et al. Neuroscience in the 21st Century. *New Tools and Techniques Driving Exciting Discoveries: Nobel Sciences*; .
 62. Marvast AF, Amnieh MH, Navabazam F, Bidaki R. The Effect of N-acetylcysteine on Alprazolam Withdrawal Symptoms in Wistar Male Albino Rats. *Cognizance Journal of Multidisciplinary Studies*. 2024;4(4):316-328.
 63. Sohrabi N, Hammoodi KA, Hammoud A, Jasim DJ, Karouei SH, Kheyri J, Nabi H. Using different geometries on the amount of heat transfer in a shell and tube heat exchanger using the finite volume method. *Case Studies in Thermal Engineering*. 2024 Mar 1;55:104037